A hair cell-specific peroxidase coordinates stomatal and prickle hair cell size to optimize epidermal cell functionality in grasses

Tiago DG Nunes[1], Magdalena W Slawinska[1], Dan Zhang[1], Leonie Redt[1], Richard Sibout[2], John P. Vogel[3,4], Barbara Jesenofsky[1], Heike Lindner[1], Michael T Raissig[1,5,*]

[1] Centre for Organismal Studies Heidelberg, Heidelberg University, Heidelberg, Germany
[2] UR1268 BIA (Biopolymères Interactions Assemblages), INRAE, Nantes, France
[3] DOE Joint Genome Institute, Berkeley, CA, USA
[4] University California, Berkeley, Berkeley, CA, USA
[5] Institute of Plant Sciences, University of Bern, Bern, Switzerland

* Address correspondence to: Michael T. Raissig E-mail: michael.raissig@ips.unibe.ch

The leaf epidermis is the outermost cell layer forming the interface between plants and the atmosphere that must accomplish contrasting functions; it must provide a robust barrier against biotic and abiotic stressors while simultaneously facilitating efficient exchange of carbon dioxide and water. To achieve these opposing requirements, the plant epidermis developed a wide range of specialized cell types such as stomata and hair cells (=trichomes). While factors forming these individual cell types are known, it is poorly understood how their number and size is coordinated. Here, we identified a role for *BdPRX76/BdPOX*, a class III peroxidase, in regulating both stomata and hair cell size in the model grass *Brachypodium distachyon*. In *bdpox* mutants stomata were longer, yet prickle hair cells were smaller. Because stomatal density remained unchanged, the negative correlation between stomatal size and density was disrupted and resulted in higher stomatal conductance and lower intrinsic water-use efficiency. Reporter lines revealed that *BdPOX* was exclusively expressed in hair cells suggesting that *BdPOX* cell-autonomously promotes hair cell size and non-cell-autonomously restricts stomatal length. Cell wall autofluorescence and lignin stainings indicated a role for *BdPOX* in lignification or crosslinking of related phenolic compounds at the hair cell base. Ectopic expression of *BdPOX* in the stomatal lineage increased phenolic content in guard cell walls and restricted stomatal elongation. Together, we reveal a developmental coordination between hair cells and stomata that optimizes epidermal functionality. We propose that a cell-type-specific disruption of this coordination leads to compensatory developmentaldefects in other epidermal cell types.

trichomes I stomata I gas exchange I grasses I *Brachypodium distachyon* I cell size I lignin I class III peroxidase

RESULTS

The spatial organization and functionality of leaf epidermal cells play fundamental roles in plant productivity and (a)biotic interactions (Dow et al., 2014; Javelle et al., 2011; Riglet et al., 2021; Zuch et al., 2022). In the model grass *B. distachyon*, the leaf blade epidermis is dominated by rectangular pavement cells, stomatal complexes, trichomes consisting of prickle hair cells (PHCs) and few interspersed macrohairs, and occasional silica cells (Fig. 1A) (Hall et al., 2020). Most specialized amongst epidermal cells are stomatal complexes, which are cellular pores on the epidermis that regulate carbon capture for photosynthesis and limit water loss. Grasses present extremely fast stomatal movements, which seem to be linked to their innovative, graminoid morphology consisting of two dumbbell-shaped guard cells (GCs) flanked by two subsidiary cells (SCs) (Franks and Farquhar, 2007; McAusland et al., 2016; Nunes et al., 2020). Fast stomatal movements and adjustments in stomatal anatomy (stomatal density and size) are crucial for water-use efficient gas exchange thereby contributing to abiotic stress resilience (Lawson and Vialet-Chabrand, 2019; Nunes et al., 2022). Still, how form and function of grass stomata are regulated remain elusive.

bdpox mutants show increased stomatal conductance and cell size defects in stomata and prickle hair cells

To identify novel factors associated with graminoid stomatal morphology and functionality, we performed RNA-sequencing of mature zones of 7 day old leaves in *B. distachyon* Bd21-3 (WT) and *bdmute* plants (Fig. S1A). The *bdmute* leaf epidermis features abnormal stomata that lack SCs which strongly affects stomatal responsiveness and gas exchange (Raissig et al., 2017). 179 genes were downregulated in *bdmute* (Table 1 in Supplementary dataset S1) and we selected ~50 candidate genes for a reverse genetic screening. Candidates were chosen according to their annotated gene function, their

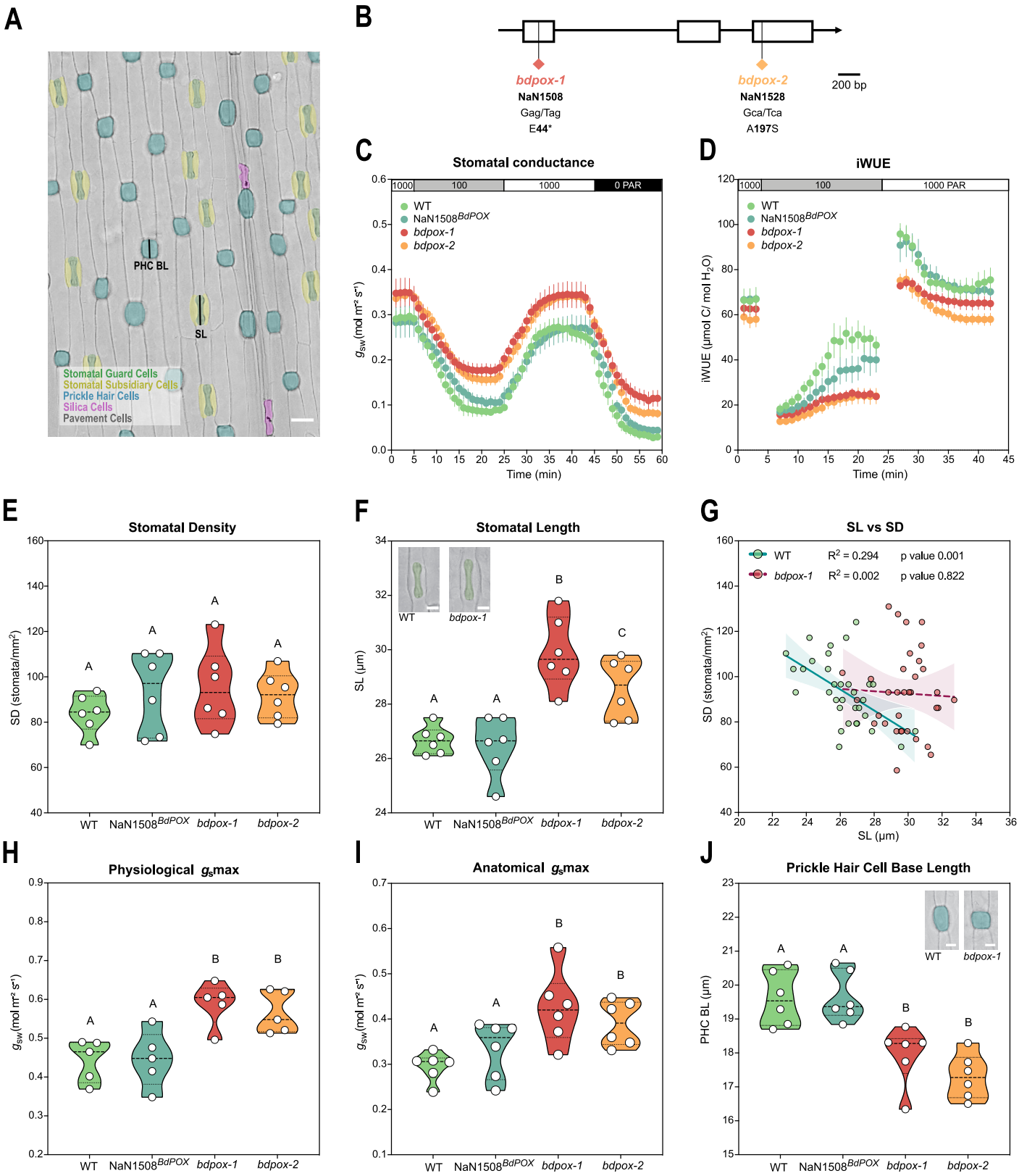

Figure 1 - *bdpox* mutants display altered gas exchange and anatomical defects in the leaf epidermis. (A) Leaf epidermis of *B. distachyon* (Bd21-3); stomatal complexes (GCs in green and SCs in yellow), prickle hair cells (blue), pavement cells (grey) and silica cells (magenta). Measuring axis of stomatal length (SL) and PHC base length (PHC BL) are indicated. Scale bar, 20 μm. **(B)** *BdPRX76/BdPOX* (BdiBd21-3.2G0467800) gene model indicating the location and nature of the mutations in *bdpox-1* (NaN1508) and *bdpox-2* (NaN1528). **(C)** Stomatal conductance (g_{sw}) in response to changing light (1000-100-1000-0 PAR) in WT, NaN1508^{BdPOX}, *bdpox-1* and *bdpox-2* (n=6 individuals per genotype). Dots represent the mean and error bars represent SEM. **(D)** Intrinsic water-use efficiency (iWUE) in response to changing light (1000-100-1000 PAR) in WT, NaN1508^{BdPOX}, *bdpox-1* and *bdpox-2* (n=6 individuals per genotype). Dots represent the mean and error bars represent SEM. **(E)** Stomatal density (SD) in WT, NaN1508^{BdPOX}, *bdpox-1* and *bdpox-2* (n=6 individuals per genotype, 548-619 stomata counted per genotype). **(F)** Stomatal length (SL) in WT, NaN1508^{BdPOX}, *bdpox-1* and *bdpox-2* (n=6 individuals per genotype; 193-287 stomata per genotype). Inset shows a DIC image of WT and *bdpox-1* stomata; GCs are false-colored in green; scale bar, 10 μm. **(G)** Correlation between average stomatal length (SL) and average stomatal density (SD) in WT and *bdpox-1* (n=33-.

expression being lower in the developmental zone (Zhang et al., 2022) and the availability of mutants from a collection of sodium azide (NaN_3) mutagenized and fully resequenced lines (Granier et al., 2016).

In the initial screen, we found that two mutants of the class III peroxidase *BdPRX76/BdPOX* (BdiBd21-3.2G0467800; Fig. 1B; S1A, B) showed lower intrinsic water-use efficiency (iWUE; Fig. S1C) and higher ambient-adapted stomatal conductance (g_{sw}; Fig. S1D). The two NaN lines disrupting *BdPRX76/BdPOX* were NaN1508, which contained a heterozygous, early STOP codon (E44*; *bdpox-1*) and NaN1528, which contained a homozygous missense mutation in the BdPOX active/heme-binding site (A197S; *bdpox-2*; Fig. 1B, S1B). From the segregating NaN1508 population, homozygous mutant individuals (*bdpox-1*, NaN1508$^{bdpox\text{-}1}$) and wild-type segregants (NaN1508^{BdPOX}) were selected by genotyping. Because NaN1508^{BdPOX} contained the same background mutations as *bdpox-1,* we included it as an additional wild-type control line.

To confirm the gas exchange defects in *bdpox* mutants, we measured stomatal conductance (g_{sw}) in response to changing light intensity (1000-100-1000-0 PAR) (Nunes et al., 2022). In *bdpox* plants, we observed higher g_{sw} in all light steps (Fig. 1C), but no significant impact on stomatal opening and closure speed (Fig. S2A-C). Since no significant variation in carbon assimilation (*A*) was observed (Fig. S2D), *bdpox* mutants suffered a decrease in intrinsic water-use efficiency (iWUE, A/g_{sw}), particularly in the light-limited step (100 PAR; Fig. 1D).

To test if the increased g_{sw} was caused by changes in stomatal density we performed microscopic analysis of the leaf epidermis from the leaves assessed for gas exchange. No differences were found regarding stomatal density (SD; Fig. 1E), yet we observed significantly longer stomata in *bdpox* mutants (Fig. 1F). This suggested that the well-established negative correlation between stomatal size and density, observed both interspecifically (de Boer et al., 2016; Doheny-Adams et al., 2012; Franks et al., 2009; Franks and Beerling, 2009; Q. Li et al., 2021; Zhang et al., 2021) and intraspecifically (Dittberner et al., 2018; Nunes et al., 2022; Sun et al., 2014), was disrupted in *bdpox* (Fig. 1G). Detailed morphometric confocal analysis of fusicoccin-treated leaves to induce full stomatal opening revealed that stomatal pores are indeed longer and larger in *bdpox* (Fig. S2F-I).

To demonstrate if the higher g_{sw} levels could be explained by the disrupted stomatal anatomy in *bdpox*, we compared physiological $g_s$max measurements with anatomical $g_s$max calculations (theoretical $g_s$max based on gas diffusion physical constants and stomatal anatomical traits) using an established equation recently optimized for grass stomata (Nunes et al., 2022). Physiological $g_s$max measurements confirmed the increased g_{sw} capacity in *bdpox* mutants (Fig. 1H), and anatomical $g_s$max calculations revealed the same relative variation between *bdpox* mutants and WT (Fig. 1I). Together, this strongly suggested a causal relationship between longer stomata and higher gas exchange in *bdpox*.

To verify if the cell size defect was specific to stomata, we also measured the length of pavement cells (PCs) and of the base of prickle hair cells (PHCs). While no differences were found in PC size among genotypes (Fig. S2J), we observed an unexpected decrease in the base length of PHCs in *bdpox* mutants (Fig. 1J).

In summary, *BdPOX* seemed to negatively regulate stomatal size but positively regulate PHC size.

BdPOX is expressed in hair cells and mutant complementation rescued stomatal and prickle hair cell phenotypes

To determine where *BdPOX* was expressed, we generated transcriptional (*BdPOXp:3xNLS-eGFP*) and translational (*BdPOXp:BdPOX-mCitrine*) reporter lines. To our surprise, both *BdPOX* reporter genes were exclusively expressed in PHCs (Fig. 2A, B; S3B, Movie S1, S2) and macrohairs (Fig. S3A). Because grass leaf development and, consequently, epidermal development follows a strict base-to-tip developmental gradient with well-established stomatal stages, we used the stomatal stages as landmarks to track PHC development (Nunes et al., 2020). We observed that both transcriptional (*BdPOXp:3xNLS-eGFP*) and translational (*BdPOXp:BdPOX-mCitrine*) reporter expression in PHCs started during stages 5-6i of stomatal development and, therefore, before significant stomatal elongation (Fig. 2A, B).

Expression of *BdPOXp:BdPOX-mCitrine* in *bdpox-1* fully complemented both the PHC and stomatal size phenotypes (Fig. 2C-E). Detailed PHC phenotyping revealed that PHC base length, area, and outgrowth which were decreased in *bdpox-1,* were rescued in three independent *bdpox-1;BdPOXp:BdPOX-mCitrine* complementation lines (Fig. 2C, D, S3C). Importantly, PHC base area was positively correlated with PHC outgrowth, indicating that PHC base measurements are a good proxy for PHC size (Fig. S3D). Stomatal length (SL) was rescued to WT levels in all three independent complementation lines (Fig. 2E) and stomatal density (SD) remained

(continued figure legend Fig. 1)
34 individuals per genotype). Linear regressions individually performed for WT (green) and *bdpox-1* (red). 95 % confidence bands are shown for WT (green) and *bdpox-1* (red). R^2 and p-values are indicated, dashed line represents non-significant correlation (slope not significantly different than zero). **(H)** Physiological $g_s$max measurements in WT, NaN1508^{BdPOX}, *bdpox-1* and *bdpox-2* (n=5 individuals per genotype). **(I)** Anatomical $g_s$max calculations in WT, NaN1508^{BdPOX}, *bdpox-1* and *bdpox-2* (n=6 individuals per genotype; same individuals as in C-F). **(J)** PHC base length in WT, NaN1508^{BdPOX}, *bdpox-1* and *bdpox-2* (n=6 individuals; 656-691 PHCs per genotype). Inset shows DIC image of WT and *bdpox-1* PHCs; PHCs false-colored in blue; scale bar, 10 μm. Different letters represent significant differences (p<0.05) obtained from one-way ANOVA followed by Tukey's multiple comparisons.

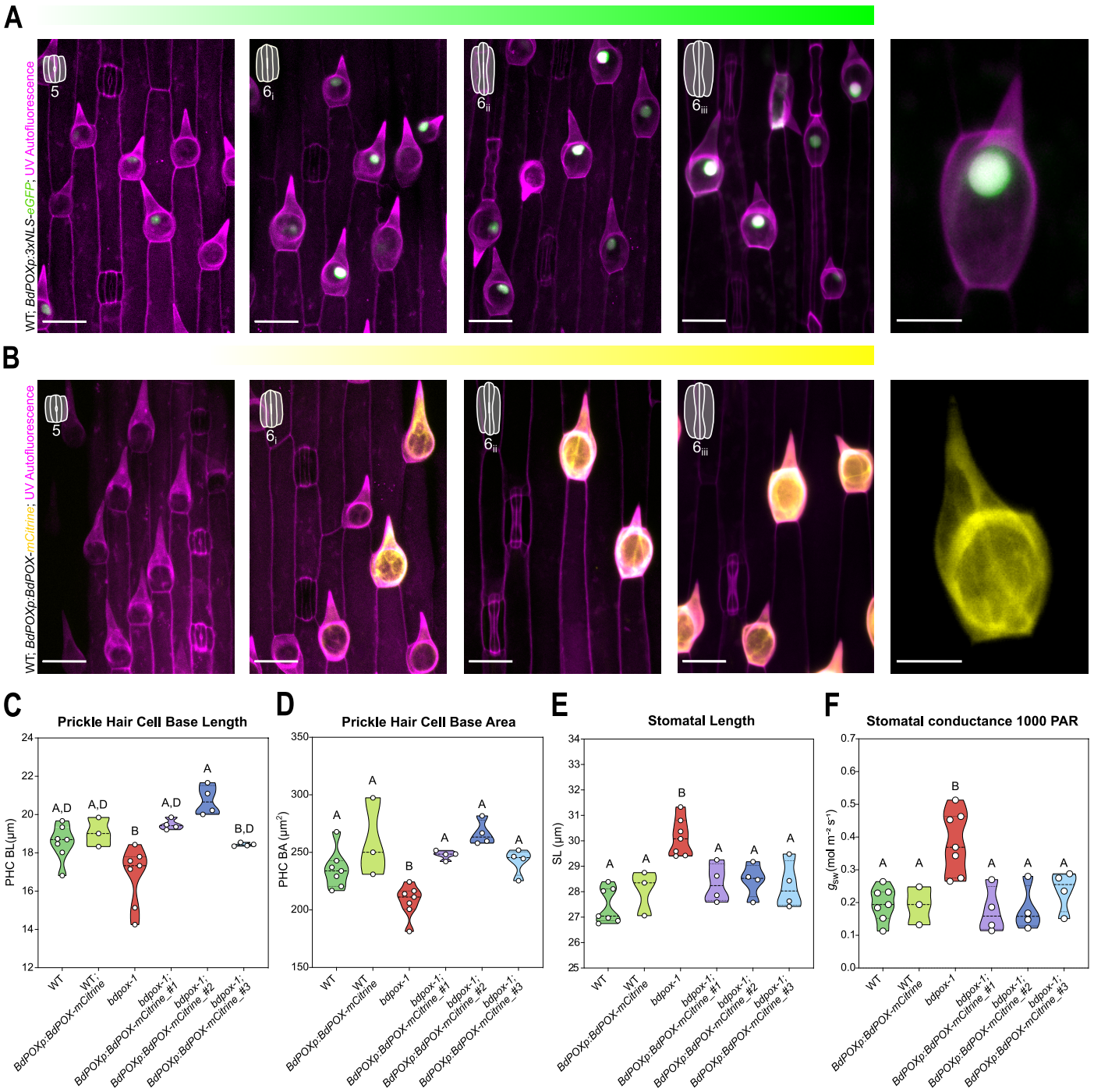

Figure 2 - *BdPOX* reporter lines are specifically expressed in hair cells and complement the anatomical and physiological defects in *bdpox-1*. **(A)** Transcriptional reporter *BdPOXp:3xNLS-eGFP* expression stages in the developing epidermis staged according to stomatal developmental stages (upper left insets); cell wall UV-induced autofluorescence indicates cell outlines (magenta). Right-most panel shows a mature PHC. **(B)** Translational reporter *BdPOXp:BdPOX-mCitrine* expression stages in the developing epidermis staged according to stomatal developmental stages (upper left insets); cell wall UV-induced autofluorescence indicates cell outlines (magenta). Right-most panel shows a mature PHC (mCitrine channel only). **(C)** PHC base length (PHC BL) in WT, *BdPOXp:BdPOX-mCitrine* (in WT), *bdpox-1* and in three independent complementation lines (*bdpox-1; BdPOXp:BdPOX-mCitrine #1, #2, #3*); n=3-7 individuals per genotype; each dot represents the average of one individual, n=160-340 PHCs per genotype/line. **(D)** PHC base area (PHC BA) in WT, *BdPOXp:BdPOX-mCitrine* (in WT), *bdpox-1* and in three independent complementation lines (*bdpox-1; BdPOXp:BdPOX-mCitrine #1, #2, #3*); n=3-7 individuals per genotype; each dot represents the average of one individual, n=128-358 PHCs per genotype/line. **(E)** Stomatal length (SL) in WT, *BdPOXp:BdPOX-mCitrine* (in WT), *bdpox-1* and in three independent complementation lines (*bdpox-1; BdPOXp:BdPOX-mCitrine #1, #2, #3*); n=3-7 individuals per genotype; each dot represents the average of one individual, n=156-355 stomata per genotype/line. **(F)** Steady-state stomatal conductance (g_{sw}) at 1000 PAR in WT, *BdPOXp:BdPOX-mCitrine* (in WT), *bdpox-1* and in three independent complementation lines (*bdpox-1; BdPOXp:BdPOX-mCitrine #1, #2, #3*); n=3-7 individuals per genotype/line. Scale bars, 20 µm (except in right-most, mature PHC panels, where scale bar is 10 µm). Different letters represent significant differences ($p<0.05$) obtained from one-way ANOVA followed by Tukey's multiple comparisons.

unaltered (Fig. S3E). Consequently, stomatal conductance (g_{sw}) was restored to wild-type levels in the complementation lines (Fig. 2F).

Ubiquitous expression of *BdPOX* in *bdpox1*, however, had no effect on cell size nor on gas exchange suggesting that a cell type-specific expression is necessary for its complementation (Fig. S3F-I).

Together, our results suggested that *BdPOX* played a cell-autonomous role in promoting PHC size and, as a consequence, non-cell autonomously restricted stomatal elongation.

BdPOX might be involved in lignification/hydroxycinnamates cross-linking at the base of prickle hair cells to positively regulate cell outgrowth

To mechanistically link how a hair-cell localized peroxidase could affect stomatal anatomy, we first investigated the cell-autonomous function of BdPOX in PHCs. The *Arabidopsis* homolog of *BdPOX*, *AtPRX66*, is associated with phenolic modifications in the cell wall, namely lignification of tracheary elements (Tokunaga et al., 2009). A unique feature of grass cell walls is the significant yet cell-type-specific amount of hydroxycinnamates (ferulic acid and ρ-coumaric acids) that are bound to arabinoxylans and/or to lignins (Coomey et al., 2020; Hatfield et al., 2016; Rancour et al., 2012; Vogel, 2008). The polymerization and crosslinking of these compounds (including monolignols into lignins) are catalyzed by laccases and/or class III peroxidases (Burr and Fry, 2009; Hoffmann et al., 2020; Le Bris et al., 2019; Rojas-Murcia et al., 2020; Wang et al., 2015). Thus, we hypothesized that BdPOX modulates PHC size by altering phenolic compounds in the cell walls.

To test this, we assessed UV-induced autofluorescence of phenolic compounds in the cell wall of PHCs (Donaldson, 2020; García-Plazaola et al., 2015; Shtein et al., 2017). PHC autofluorescence plot profiles and corrected total cell fluorescence revealed lower autofluorescence in *bdpox-1* compared to WT and complemented *bdpox-1*, specifically at the base of the PHCs (approximately the initial 12 µm; Fig. 3A-C, S4A).

To test if the lower cell wall autofluorescence originated from decreased lignin/hydroxycinnamates content, we used different histochemical stainings. Basic fuchsin is a standard lignin stain (Holzwart et al., 2018; Sexauer et al., 2021; Ursache et al., 2018) that also has a high affinity for hydroxycinnamates in the *B. distachyon* cell wall (Kapp et al., 2015). Simultaneous imaging of cell wall autofluorescence and fuchsin-stained lignin showed that fuchsin preferentially stained the lower section of PHCs while total phenolics autofluorescence was observed until the tip (Fig. 3D- F; Movie S3, Movie S4). Indeed, *bdpox-1* mutants showed lower fuchsin fluorescence intensity at the basal section of PHCs (first 12 µm from the basal outline) compared to WT and complemented *bdpox-1* lines (Fig. 3F, G; Movie S3-S5) suggesting reduced lignin/hydroxycinnamates content in the mutant. Very similar results were observed using safranin-O lignin staining (Fig. S4B, C), in which increased red fluorescence is observed in lignified cells, whereas non-lignified cell walls preferably fluoresce in green (Bond et al., 2008). Therefore, a red/green ratiometric analysis allows for a semi-quantitative evaluation of cell wall lignification (Baldacci-Cresp et al., 2020). *bdpox-1* mutants displayed a lower safranin-o ratio at the base section of PHCs (first 12 µm) compared to WT and complemented *bdpox-1*, again indicating a decrease in lignin content in the mutant (Fig. S4B, C).

Regarding stomata, no significant differences were observed in autofluorescence nor in fuchsin-stained lignin in mature GCs between WT and *bdpox-1* (Fig. S4D, E). When looking at the developing stomata during stomatal elongation/maturation, we observed that cell wall autofluorescence increased in wild-type GCs (Fig. S4F). This increase appeared to start earlier in *bdpox-1* but stalled sooner, too, which may be linked to the stomatal elongation defects in the mutants (Fig. S4F).

Overall, our data suggests that *BdPOX* participates in lignification of the basal cell wall of PHCs, which seems to be required for proper PHC growth, and indirectly impacts stomatal elongation.

Specific expression of *BdPOX* in the stomatal lineage arrests stomatal elongation

BdPOX appeared to be involved in cell wall phenolic modifications (lignification/crosslinking) at the base of PHCs to promote cell growth. How this PHC-specific process, however, affected stomatal elongation remained elusive. When following the basipetal developmental gradient of the *B. distachyon* epidermis, we found that PHCs grow and mature significantly before the stomatal complexes start to elongate (Fig. 4A). PHC outgrowth started when stomata were in early stages of development (i.e. stage 3-4 during SC recruitment) and was completed before GCs elongated and acquired the mature dumbbell morphology (Fig. 4A). Therefore, the growth restriction of PHCs in *bdpox* could secondarily influence stomatal anatomy, but not *vice versa*. Accordingly, the ectopic expression of *BdPOX* in the developing GC lineage using a stomatal-lineage specific promoter (*BdMUTEp:BdPOX(CDS)-mCitrine*; Fig. 4B) significantly restricted stomatal elongation in *bdpox-1*, which correlated with increased phenolics autofluorescence in GCs (Fig. 4C, D). PHC size, however, remained unaffected (Fig. 4E) as PHCs matured before stomata elongated. Intriguingly, we observed aberrant cell divisions in the pavement cells surrounding stomata when expressing *BdMUTEp:BdPOX(CDS)-mCitrine* in *bdpox-1* (Fig. 4F, G). This suggested that elongating stomata might compensate for tissue-wide mechanical imbalances caused by too small PHCs in the *bdpox-1* epidermis. Thus, when ectopic, stomatal lineage-specific expression of *BdPOX* inhibited compensato-

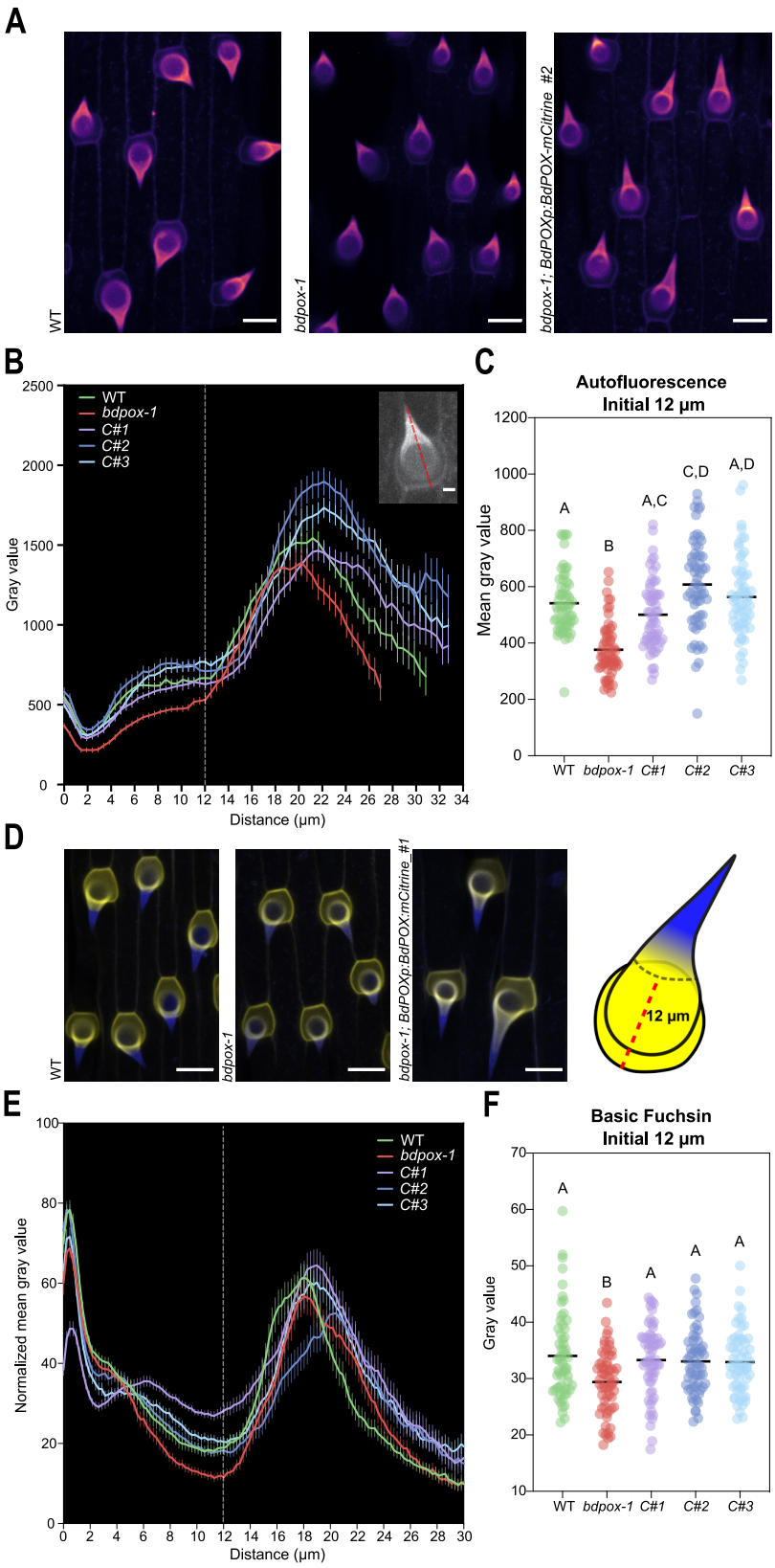

Figure 3 - *BdPOX* affects cell wall phenolic content through lignification and/or hydroxycinnamates crosslinking
(A) Cell wall autofluorescence of the mature epidermis in WT, *bdpox-1* and in *bdpox-1; BdPOXp:BdPOX-mCitrine #2*. Scale bar, 20 µm. **(B)** Average plot profiles of cell wall autofluorescence in PHCs in WT, *bdpox-1* and three complementation lines (*bdpox-1; BdPOXp:BdPOX-mCitrine #1, #2, #3);* n=60 PHCs per genotype. Error bars represent SEM. Scale bar, 5 µm. **(C)** Average cell wall autofluorescence of the initial 12 micrometers of the PHCs in WT, *bdpox-1* and three complementation lines (*bdpox-1; BdPOXp:BdPOX-mCitrine #1, #2, #3);* n=60 PHCs per genotype. **(D)** Simultaneous imaging of phenolics autofluorescence (blue) and fuchsin-stained lignin (yellow) in WT, *bdpox-1* and *bdpox-1*; *BdPOXp:BdPOX-mCitrine #1*. Scale bars, 20 µm. **(E)** Average plot profiles of fuchsin-stained lignin in PHCs of WT, *bdpox-1* and three complementation lines (*bdpox-1; BdPOXp:BdPOX-mCitrine #1, #2, #3);* n=60 PHCs per genotype. Error bars represent SEM. **(F)** Basic fuchsin stain fluorescence in the initial 12 µm of the PHCs in WT, *bdpox-1* and three complementation lines (*bdpox-1; BdPOXp:BdPOX-mCitrine #1, #2, #3);* n=60 PHCs per genotype. Different letters represent significant differences ($p<0.05$) from one-way ANOVA followed by Tukey's multiple comparisons.

ry stomatal elongation in the *bdpox-1*, additional divisions in pavement cells around stomata might be triggered to compensate for these tissue-wide mechanical tensions instead.

In conclusion, ectopically expressed *BdPOX* in GCs can modify phenolic cell wall content and modulate cell size. We propose that the size of stomata and PHCs must be coordinated for optimal epidermal functionality and that disturbing this coordination leads to compensatory developmental defects.

DISCUSSION

The leaf epidermis is the barrier between the inner photosynthetically active tissues and the environment. Highly specialized epidermal cell types facilitate the contrasting functional requirements of this outermost barrier like preventing desiccation, enabling gas exchange or deterring herbivores. Stomata, for example, open to enable carbon dioxide uptake and close to limit water loss. Trichomes, on the other hand, protect the leaf from (a)biotic stressors (Javelle et al., 2011). Several studies suggest that trichome patterning intersects with the core stomatal developmental programs in *Arabidopsis* (Adrian et al., 2015; Kanaoka et al., 2008; Torii, 2021; Yan et al., 2014). Also in grasses, failing to specify stomatal identity results in hair cells being formed in their place in *B. distachyon* (Raissig et al., 2016) and failing to specify hair cell identity leads to ectopic stomata in maize (Kong et al., 2021). This suggests that these cell types are ontogenetically closely related in grasses and that their development is thus likely coordinated. Furthermore, stomatal and trichome densities were shown to be negatively correlated in *Solanum lycopersicum*. The stomata to trichome ratio determined water-use efficiency (Galdon-Armero et al., 2018) suggesting a physiological relevance for the coordination between the two cellular features. Yet, the mechanisms that coordinate the formation and growth of stomata and trichomes remain highly unexplored.

Many core players guiding grass stomatal de-

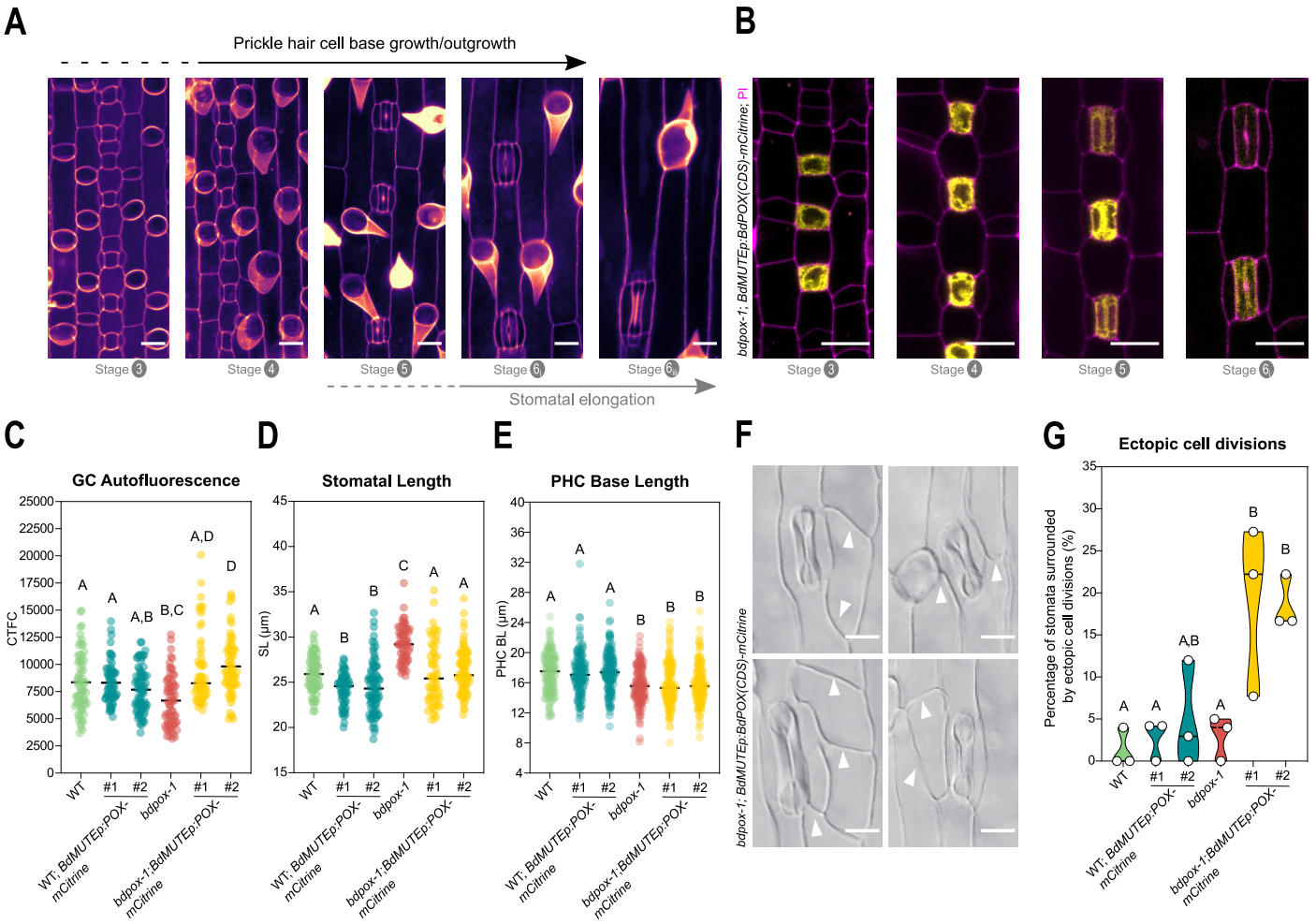

Figure 4 - Guard cell-specific expression of *BdPOX* inhibits stomatal elongation and indicates a tissue-wide, compensatory cell elongation mechanism.

(A) Stages of prickle hair cell development and respective stomatal development stages (gray; stage 3 - 6). PHC differentiation, outgrowth and morphogenesis starts when the stomatal lineages are still dividing and concludes before stomatal complexes are fully elongated. Scale bars, 10 µm. **(B)** *BdMUTEp:BdPOX(CDS)-mCitrine* expression in the developing GC lineage. *BdPOX(CDS)-mCitrine* expression in GMCs (stage 3), GMCs after SC recruitment (stage 4), early developing GCs (stage 5) and early elongating GCs (stage 6i; from left to right). Scale bar, 10 µm. **(C)** Quantification of cell wall autofluorescence (corrected total cell fluorescence) of GCs (n=59-75 stomata per genotype) in 2nd leaves from WT, *bdpox-1* and *BdMUTEp:BdPOX(CDS)-mCitrine* lines expressed in WT and *bdpox-1*. **(D)** Quantification of stomatal length (n=61-81 stomata per genotype) in mature leaves from WT, *bdpox-1* and *BdMUTEp:BdPOX(CDS)-mCitrine* lines expressed in WT and *bdpox-1*. **(E)** Quantification of PHC base length in mature leaves from WT, *bdpox-1* and *BdMUTEp:BdPOX(CDS)-mCitrine* lines expressed in WT and *bdpox-1* (n=140-152 PHCs per genotype). **(F)** Ectopic cell divisions per stomata when *BdMUTEp:BdPOX(CDS)-mCitrine* is expressed in *bdpox-1*. Scale bars, 10 µm. **(G)** Quantification of the percentage of stomata showing ectopic cell divisions in their neighboring pavement cells in mature leaves of WT, *bdpox-1* and *BdMUTEp:BdPOX(CDS)-mCitrine* expressed in WT and *bdpox-1* (n=3 individuals per genotype/line; 66-88 stomata per genotype/line). Different letters represent significant differences ($p<0.05$) obtained from one-way ANOVAs followed by Tukey's multiple comparisons.

velopment were characterized (Abrash et al., 2018; Cartwright et al., 2009; Facette et al., 2015; Humphries et al., 2011; Jangra et al., 2021; Liu et al., 2009; Nunes et al., 2020; Raissig et al., 2017, 2016; Wang et al., 2019; Wu et al., 2019), whereas hair cell formation remains poorly explored (Torii, 2021). Few grass trichome initiation factors such as the transcription factors HAIRY LEAF 6 (HL6) (Fei et al., 2020; Sun et al., 2017)(Angeles-Shim et al., 2012; Sun et al., 2017) and SQUAMOSA PROMOTER BINDING PROTEIN-LIKE 10/14/26 (SPL10/14/26) (Kong et al., 2021)(Lan et al., 2019; J. Li et al., 2021) were identified in rice and maize, but factors that affect morphogenesis and size remain mostly unknown. Here, we identified *BdPOX* and revealed its role in coordinating PHC and stomatal size for optimal water-use efficiency in the model grass *B. distachyon*. *BdPOX* was exclusively expressed in the hair cells and seemed to participate in the lignification or/and cross-linking of cell wall phenolics (such as hydroxycinnamates) specifically at the base of PHCs. Since lignin is a cell wall polymer that provides mechanical support (Li et al., 2009; Rogers and Campbell, 2004; Zhao et al., 2020) we suggest that such cell wall modifications at the base of PHCs are required to increase tensile strength and provide physical support for cell outgrowth.

The reduction in PHC size in *bdpox* non-cell-autonomously altered stomatal size, but did not translate to changes in stomatal density. The resulting disruption of the negative correlation between stomatal size and density likely has two

reasons; first, changes to stomatal size occur much later in development than the determination of stomatal density. Thus, changes in stomatal density can affect stomatal size *a posteriori*, where an increase in stomatal numbers can induce a downstream effect on the cell-wall machinery controlling stomatal elongation. This process is very unlikely to happen in the other direction particularly in grasses, where early stages are not only temporally but also spatially separated from late stages. Second, *bdpox* primarily impacts the PHC lineage and only affects stomatal development as a secondary consequence. Without a disruption of the stomatal genetic toolbox itself it is unlikely that a compensatory mechanism could be induced in a timely manner.

However, the exact mechanism of how restricting PHC growth induces stomatal elongation remains vague. We speculate that decreased PHC size may lead to changes in mechanical and/or geometrical constraints in the epidermal tissue, which would allow for increased stomatal elongation as a compensatory mechanism to reconstitute the tensile balance in the epidermis. The increase in stomatal length observed in *bdpox* mutants (~9 %) was quantitatively equivalent to the decrease in PHC base length (~10 %). In addition, expressing *BdPOX* in the GC lineage of *bdpox-1* resulted in an epidermis containing both shorter stomata and shorter PHCs and induced aberrant cell divisions surrounding the stomatal complexes. We speculate that the combination of restricted PHC growth due to *bdpox-1* and a prevention of stomatal elongation due to GC-expressed *BdPOX* may have caused a mechanical imbalance in the elongating epidermis resulting in cell divisions to compensate cellular tensions particularly around stomatal complexes. Alternatively, changes in hydrogen peroxide levels in the PHC apoplast due to loss of *BdPOX* might affect the reactive oxygen species signaling landscape, which could influence stomatal length non-cell-autonomously.

Regardless, the unique disruption in the negative correlation between stomatal size and density allowed us to investigate how modifying a single stomatal anatomical trait (i.e. stomatal size) would affect gas exchange. While an increase in stomatal size enhanced stomatal conductance, it did not significantly affect stomatal opening and closing speed, corroborating our previous observation that stomatal speed was correlated with stomatal density but not with stomatal size in *B. distachyon* (Nunes et al., 2022).

Overall, we identified a hair cell marker that coordinates stomata and PHC formation for optimal leaf epidermal functionality. In addition, *BdPOX* provides a novel tool to explore the molecular identity of PHCs and help to further elucidate the developmental and functional interplay between PHCs and stomata. We highlight a way to change length, cell-wall composition, and potentially even stiffness of grass trichomes that are of major relevance for biotic and abiotic interactions, namely in protection against herbivory and high sun irradiance (Andama et al., 2020; González Moreno et al., 2022; Hall et al., 2020; Karabourniotis et al., 2020). Finally, we revealed an unexpected, indirect route to engineer stomatal size in grasses without affecting stomatal density by changing cell wall properties and growth of PHCs.

DATA AND CODE AVAILABILITY

All gas exchange and microscopic quantifications used in this study can be found in Supplementary Dataset S2. Raw and processed RNA-sequencing data are available at Gene Expression Omnibus (GEO) with the accession number GSE206682. Images are available upon request.

ACKNOWLEDGMENTS

The authors thank Prof. Dr. Annika Guse and Prof. Dr. Jochen Wittbrodt for access to microscope facilities, Prof. Dr. Karin Schumacher, Prof. Dr. Rüdiger Hell, Dr. Upendo Lupanda, and Dr. Paula Ragel for the scientific and technical insights and encouragement on the development of the project. We furthermore thank Michael Schilbach for managing the greenhouse and for gardening support. We would also like to acknowledge Prof. Dr. Dominique C. Bergmann and the Howard Hughes Medical Institute for supporting the RNA-sequencing experiment and Laura R. Lee for help with RNA-seq data analysis. This research was supported by the German Research Foundation (DFG) Emmy Noether grant RA 3117/1-1 (to M.T.R.) and seed funding of the CRC1101 "Molecular Coding of Specificity in Plant Processes" (to M.T.R).

AUTHORS CONTRIBUTION

T.D.G.N. and M.T.R conceived and designed the research. M.T.R. performed and analyzed the RNA-seq data. T.D.G.N. performed the experiments and data analysis. M.W.S. performed the confocal morphological characterization of *bdpox-1* stomatal pores and the measurements of GC autofluorescence during stomatal elongation. D.Z. helped establish the confocal imaging of prickle hair cell developmental stages and prepared the slides for the blinded phenotyping of complementation experiments. R.S. and J.V. generated and provided NaN mutant lines. L.R. genotyped and selected *bdpox-1* and NaN1508^{BdPOX}. H.L. and B.J. performed the embryo isolation, calli induction, culture and transformation. H.L., B.J. and T.D.G.N. performed the selection, regeneration and screening of transgenic plants. T.D.G.N., M.W.S., D.Z., H.L. and M.T.R. contributed to data visualization and interpretation. T.D.G.N., H.L and M.T.R. wrote the manuscript. All authors commented on and edited the manuscript.

DECLARATION OF INTERESTS

The authors declare no potential conflicts of interest.

SUPPLEMENTARY MATERIALS

Figures S1-S4

Movie S1: *BdPOX* translational reporter (*BdPOXp:BdPOX-mCitrine*).

Movie S2: *BdPOX* transcriptional reporter (*BdPOXp:3xNLS-eGFP*).

Movie S3: Prickle hair cells' autofluorescence and basic fuchsin staining in WT.

Movie S4: Prickle hair cells' autofluorescence and basic fuchsin staining in *bdpox-1*.

Movie S5: Prickle hair cells' autofluorescence and basic fuchsin staining in *bdpox-1; BdPOXp:BdPOX-mCitrine_#1*.

Supplementary Dataset 1: RNA-seq data (DEG list) and list of primers used.

Supplementary Dataset 2: Leaf-level gas exchange data, anatomical data from light and confocal microscopy and data from histochemical experiments (autofluorescence and lignin stainings).

MATERIAL AND METHODS

Transcriptional profiling of WT and *bdmute* leaves by RNA-sequencing

25 mature leaf zones (25-30 mm from the base of 2nd leaves) per replicate were collected from three wild-type (Bd21-3) replicates and from three *bdmute* replicates (7 days after germination seedlings grown on ½ MS plates at 20°C with ~100 µmol photons m^{-2} s^{-1} light) were carefully collected, snap-frozen in liquid nitrogen and grounded using mortar and pistil. RNA extraction, library preparation, RNA-sequencing and data analysis was essentially performed as described in (Zhang et al., 2022). To be specific, total RNA was isolated using Qiagen's RNeasy Plant Mini kit with on-column DNAse digestion according to the manufacturer's instructions. The Kapa mRNA HyperPrep (Roche) was used to generate an mRNA enriched sequencing library with an input of 1µg of total RNA. The libraries were sequenced using the Illumina NextSeq500 platform. Read quality was assessed with FastQC and mapped against the Bd21-3v1.0 genome using bowtie2. Mapped reads were counted using summarized overlap and differentially expressed genes were analyzed using DeSeq2. Finally, gene expression was normalized by transcripts per kilobase million (TPM). Raw and processed data are available at Gene Expression Omnibus (GEO) with the accession number GSE206682.

Plant Material and Growth Conditions

The *B. distachyon* line Bd21-3 was used for all experiments. The *bdpox* mutant lines (*bdpox-1*, NaN1508 and *bdpox-2*, NaN1528) were obtained from the Sodium Azide (NaN_3) mutagenized population (NaN lines) that was fully resequenced. NaN1508 contained a heterozygous early STOP mutation. Homozygous lines (*bdpox-1*, NaN1508$^{bdpox-1}$) and wild-type-like lines (NaN1508^{BdPOX}) were selected by PCR amplifying the variant containing region using priTN88/priTN89 followed by Sanger sequencing.

Seeds were sterilized for 15 min with 20% bleach and 0.1% Tween, thoroughly rinsed, stratified on MS plates (½ MS (Caisson Labs), 1% Agar (w/v), pH 5.7) for 2 days at 4°C before transfer to a 28°C growth chamber with 16h light:8h dark cycle (110 µmol photons m^{-2} s^{-1}) or directly transferred to soil (Haas and Raissig, 2020).

Growth conditions for *B. distachyon* are specified in (Nunes et al., 2022). In short, plants on soil were grown in a greenhouse with 18h light:6h dark cycle (200-400 µmol m^{-2} s^{-1}; day temperature = 28°C, night temperature = 22°C).

Reporter Constructs

Reporter and overexpression constructs were generated using the Greengate cloning system (Lampropoulos et al., 2013). *BdPOX* promoter and coding sequences were ampli-

fied from wild-type *Brachypodium distachyon* (Bd21-3) genomic DNA extracted using a standard CTAB DNA extraction protocol (Allen et al., 2006) and from cDNA synthesized with the RevertAid First Strand cDNA Synthesis Kit (Cat. No.: K1621); ThermoFisher Scientific, Massachusetts, USA) from RNA extracted with the RNeasy Micro Kit (Cat. No.: 74004; Qiagen, Hilden, Germany).

To clone the *BdPOX* genomic sequence, a point mutation was induced in the genomic *BdPOX* sequence to eliminate a BsaI/Eco31I site (GGTCTC) in the second intron. Genomic *BdPOX* was amplified in two separate fragments using priTN99/priTN102 and priTN100/priTN101 (containing the bp substitution **A**GTCTC). The two resulting PCR products were purified using the NucleoSpin Gel and PCR Clean-up kit (Ref. REF 740609.50; Macherey-Nagel, Düren, Germany), digested at 37°C overnight using FastDigest Eco31I (Thermo Fisher Scientific, Waltham, Massachusetts, USA) and ligated overnight at 16°C using T4 ligase (NEB, Ipswich, Massachusetts, USA). The fully reassembled *BdPOX* gene was ligated overnight at 16°C with the previously digested (FastDigest Eco31I) and dephosphorylated pGGC000 entry vector (with Antarctic Phosphatase, NEB) to generate *pGGC_BdPOX*. *BdPOX (CDS)* sequence was amplified using priTN99/priTN100 from cDNA. The resulting PCR product was purified and digested using FastDigest Eco31I (Thermo Fisher Scientific), and ligated using T4 ligase (NEB) with previously digested (FastDigest Eco31I) and dephosphorylated (Antarctic Phosphatase) pGGC000 entry vector to generate *pGGC_BdPOX(CDS)*.

To clone the *BdPOX* promoter, a 3.5kb region upstream of the *BdPOX* transcriptional start site was amplified using priTN95/priTN96. The PCR product was purified and digested using FastDigest Eco31I (Thermo Fisher Scientific) and ligated using T4 ligase (NEB) with previously digested (FastDigest Eco31I) and dephosphorylated (Antarctic Phosphatase) pGGA000 entry vector to generate *pGGA_BdPOXp*. The constitutive *ZmUbi* promoter was amplified from *pEX_BdMUTEp:CitYFP-BdMUTE (Raissig et al., 2017)* with priTN3/priTN4 and cloned into pGGA000 (*pGGA_ZmUbip*). The *BdMUTE* promoter was amplified from *pEX_BdMUTEp:CitYFP-BdMUTE* (Raissig et al., 2017) with priTN1/priTN28 and priTN2/priTN29 (containing a bp substitution GA**T**ACC to mutate a BsaI site) and cloned into pGGA000 (*pGGA_BdMUTEp*). The PvUbip-driven hygromycin resistance cassette was amplified from *pTRANS_250d* (Čermák et al., 2017) using priTN11/priNT30 and priTN12/priTN29 (containing a 1 bp substitution GA**T**ACC to mutate a BsaI in the *PvUbi2* promoter sequence), and cloned into pGGF000 (*pGGF_PvUBi2p:HygR*). All constructs were test digested and Sanger sequenced to verify that the appropriate sequence was yielded.

The entry modules pGGB003 (B-dummy), pGGD002 (D-dummy) and pGGE001 (rbcS terminator) are described in (Lampropoulos et al., 2013). The entry modules *pGGB_3xNLS* and *pGGC_eGFP* were generously provided by Prof. Dr. Karin Schumacher's group. The pGGD009 (Linker-mCitrine) was generously provided by Prof. Dr. Jan Lohmann's group.

BdPOXp:BdPOX-mCitrine, *ZmUbip:BdPOX:mVenus*, *ZmUbip:BdPOX(CDS)-mCitrine*, *BdMUTEp:BdPOX(CDS)-mCitrine* and *BdPOXp:3xNLS-eGFP* were generated using the Green Gate assembly (Lampropoulos et al., 2013). In short, the 6 different entry modules (pGGA_specific promoter; pGGB_dummy or N-tag; pGGC_gene sequence or tag; pGGD_dummy or C-tag; pGGE_terminator and pGGF_resistance) were repeatedly digested and ligated with the destination vector pGGZ004 during 50 cycles (5 min 37°C followed by 5 min 16°C) followed by 5 min at 50°C and 5 min at 80°C for heat inactivation of the enzymes. All final constructs were test digested and the generated GreenGate overhangs were Sanger sequenced.

Generation and Analysis of Transgenic Lines

Embryonic calli derived from Bd21-3 and *bdpox-1* parental plants were transformed with AGL1 *Agrobacterium tumefaciens* containing the binary expression vectors, selected based on hygromycin resistance, and regenerated as described in (Zhang et al., 2022). In short, young, transparent embryos were isolated and grown for three weeks on callus induction media (CIM; per L: 4.43g Linsmaier & Skoog basal media (LS; Duchefa #L0230), 30g sucrose, 600µl CuSO4 (1mg/ml, Sigma/Merck #C3036), 500µl 2,4-D (5mg/ml in 1M KOH, Sigma/Merck #D7299), pH 5.8, plus 2.1g of Phytagel (Sigma/Merck #P8169)). After three weeks of incubation at 28°C in the dark, crisp, yellow callus pieces were subcultured to fresh CIM plates and incubated for two more weeks at 28°C in the dark. After two weeks, calli were broken down to 2-5mm small pieces and subcultured for one more week at 28°C in the dark. For transformation, AGL1 Agrobacteria with the desired construct were dissolved in liquid CIM media (same media as above without the phytagel) with freshly added 2,4-D (2.5µg/ml final conc.), Acetosyringone (200µM final conc., Sigma/Merck #D134406), and Synperonic PE/F68 (0.1% final conc., Sigma/Merck #81112). The OD600 of the Agrobacteria solution was adjusted to 0.6. Around 100 calli were incubated for at least 10min in the Agrobacteria solution, dried off on sterile filter paper and incubated for three days at room temperature in the dark. After three days, transformed calli were moved to selection media (CIM + Hygromycin (40µg/ ml final conc., Roche #10843555001) + Timentin (200µg/ ml final conc., Ticarcillin 2NA & Clavulanate Potassium from Duchefa #T0190)) and incubated for one week at 28°C in the dark. After one week, calli were moved to fresh selection plates and incubated for two more weeks at 28°C in the dark. Next, calli were moved to callus regeneration media (CRM; per L: 4.43g of LS, 30g maltose (Sigma/Merck #M5885), 600µl CuSO4 (1mg/ml), pH 5.8, plus 2.1g of Phytagel). After autoclaving, cool down and add Timentin (200µg/ml final conc.), Hygromycin (40µg/ml final conc.), and sterile Kinetin solution (0.2µg/ml final conc., Sig-

ma/Merck #K3253). Calli were incubated at 28°C and a 16h light:8h dark cycle (70-80 µmol PAR m^{-2} s^{-1}). After 1-6 weeks in the light, shoots will form. Move shoots that are longer than 1cm and ideally have two or more leaves, to rooting cups (Duchefa #S1686) containing rooting media (per L: 4.3g Murashige & Skoog including vitamins (Duchefa #M0222), 30g sucrose, adjust pH to 5.8, add 2.1g Phytagel). After autoclaving, cool down and add Timentin (200µg/ml final concentration). Once roots have formed, plantlets can be moved to soil (consisting of 4 parts ED CL73 (Einheitserde) and 1 part Vermiculite) and grown in a greenhouse with 18h light:6h dark cycle (250-350 µmol PAR m^{-2} s^{-1}). Ideally, the transgenic plantlets moved to soil are initially kept at lower temperatures (day temperature = 22°C, night temperature = 18-20°C) for 2-4 weeks until they have rooted sufficiently before being moved to the warmer greenhouse (day temperature = 28°C, night temperature = 22°C).

We refer to *Brachypodium* regenerants as T0 and to the first segregating population as T1. We analyzed 5-10 independent lines in the T0 generation (depending on how many independent lines were recovered upon regeneration). We confirmed the observed expression pattern and performed the phenotyping studies using one to three independent and fertile T0 transgenics that produced seeds (3-4 T1 individuals per line).

Gas exchange phenotyping

Infra-red gas analyser-based leaf-level gas exchange measurements were performed as described in (Nunes et al., 2022). All measurements were performed on the youngest fully expanded mature leaf of *B. distachyon* plants 3 weeks after sowing (17-24 days after sowing) using a LI-6800 (LI-COR Biosciences Inc, Lincoln, NE, USA). Ambient light intensity was monitored during the measurements using an external LI-190R PAR Sensor attached to LI-6800. Greenhouse temperature and relative humidity were monitored during the experiments using an Onset HOBO U12-O12 4-channel data logger that was placed next to the plants used for analysis.

Light response kinetics: LI-6800 chamber conditions were as follows: flow rate, 500 µmol s^{-1}; fan speed, 10000 rpm; leaf temperature, 28° C; relative humidity (RH), 40 %; [CO_2], 400 µmol mol^{-1}; photosynthetic active radiation (PAR), 1000 – 100 – 1000 – 0 µmol PAR m^{-2} s^{-1} (20 min per light step). Gas exchange measurements were automatically logged every minute. The leaf section measured inside the LI-6800 chamber was collected, fixed and cleared to measure leaf area and accurately determine A and g_{sw} and stomatal anatomical parameters like stomatal length and density. iWUE was calculated as the ratio of A to g_{sw}. Stomatal opening and closure speed were evaluated by rate constants (k, min^{-1}) determined from exponential equations fitted for each of the three light transitions (1000-100, 100-1000 and 1000-0 PAR), as described in (Nunes et al., 2022).

Maximum stomatal conductance: Maximum stomatal conductance (physiological $g_s$max) measurements were performed with the following LI-6800 conditions: flow rate, 500 µmol s^{-1}; fan speed, 10000 rpm; leaf temperature, 28°C; relative humidity (RH), 68-70 %; [CO_2], 100 µmol mol^{-1}; PAR, 1500 µmol PAR m^{-2} s^{-1}. Gas exchange measurements were automatically logged every minute and physiological $g_s$max was calculated as the average of the last 5 min at steady-state.

Anatomical $g_s$max calculations: Anatomical $g_s$max calculations were performed on the 6 individuals for which gas exchange and stomatal anatomy was assessed (Fig. 1D-G). Based on the formula optimized for *B. distachyon* in (Nunes et al., 2022) this requires the measurement of three anatomical parameters: stomatal length, stomatal density and GC width at the apex (average of 30 stomata per individual) from images obtained using a Leica DM5000B microscope.

Steady-state stomatal conductance: LI-6800 chamber conditions were as follows: flow rate, 500 µmol s^{-1}; fan speed, 10000 rpm; leaf temperature, 28°C; relative humidity (RH), 40 %; [CO_2], 400 µmol mol^{-1}; photosynthetic active radiation (PAR), 1000 PAR m^{-2} s^{-1} (20 min). Gas exchange measurements were automatically logged every minute. The leaf section measured inside the Li-6800 chamber was collected to measure leaf area to accurately determine A and g_{sw} and, then fixed and cleared to determine stomatal anatomical parameters like stomatal length and density. All measurements were performed in a semi-randomized manner between 11:30 and 17:30 h to assure measurements for each genotype covered identical periods of time of the day and to avoid the influence of the diurnal variation of g_{sw} observed in (Nunes et al., 2022).

Ambient-adapted stomatal conductance: Steady-state ambient-adapted stomatal conductance was assessed using a SC-1 porometer (Meter, Pullman, Washington, USA). SC-1 was calibrated using the calibration plate and the moist circular filter paper provided with the SC-1. Each measurement was performed in automode (30 s). The relative humidity of the SC-1 porometer was returned to < 10 % after each measurement by shaking the sensor head for 30-90 s. Three to four fully expanded leaves per individual were measured twice. Three *B. distachyon* (Bd21-3) and three *bdpox-1* individuals were assessed three weeks after sowing. All measurements were performed in a randomized manner between 8:00 and 9:30 h, to avoid the influence of the diurnal variation of g_{sw} observed in (Nunes et al., 2022).

Important note: Some of the wild-type gas exchange measurements were previously published in (Nunes et al., 2022), where 120 wild-type measurements over the course of 2 years were correlated to variable growth conditions. The WT gas exchange data that was published in (Nunes et al., 2022) is

indicated accordingly in the Supplementary Dataset 2.

Microscopy and Phenotypic Analysis

Most of the morphometric and the cell wall measurements were performed on the actual leaf segments used for gas exchange measurement to thoroughly link cellular form and composition to stomatal gas exchange.

Leaf epidermis morphometry: For DIC imaging, the youngest fully expanded mature leaves (3 weeks after sowing) were collected after LI-6800 measurements and placed into 7:1 ethanol:acetic acid and incubated overnight to fix the leaf tissue and remove chlorophyll. To prepare samples for imaging, the tissue was rinsed twice in water, mounted on slides in Hoyer's solution (Sharma, 2017) and the abaxial side was examined using a Leica DM5000B microscope (Leica Microsystems, Wetzlar, Germany). Typically, 4-6 (40x objective) and 3-5 (20x objective) abaxial fields of view per leaf of each individual plant were imaged to determine stomatal length, stomatal density, stomatal width at the apices, pavement cell length, prickle hair cell (PHC) base length, base area and/or PHC outgrowth using the straight line tool xyz and/or the polygon selection tool in Fiji (Schindelin et al., 2012). In the case of complementation experiments represented in Figure 2, the slides were prepared and randomized by an independent researcher before measurements on Fiji, to avoid potential biased phenotyping. The confocal morphometrical analysis of stomata in Bd21-3 and *bdpox-1* mutants, were performed as described in (Nunes et al., 2022). Leaves were incubated overnight in buffer solution (50mM KCl, 10mM MES-KOH) with 4mM Fusicoccin (Santa Cruz Biotechnology, Inc., Dallas, TX, USA; Cat. no. 20108-30-9) in the light to force stomatal opening. Leaves were stained in propidium iodide (Sigma-Aldrich, St. Louis, Missouri, USA, Cat. no. P3566; PI, 1:100 of a 1 mg/ml stock) for 5 min and Z-stacks were taken using confocal microscopy. Image analysis was done using Fiji to measure stomatal pore length and stomatal pore area (hand-traced).

Stomatal associated-epidermal defects: Stomata and stomata surrounded by defective cell divisions were counted in 5 abaxial fields of view (40 x objective) per leaf of each individual plant. Finally the percentage of stomatal-associated defects was calculated as the total number of stomata surrounded by defective cell divisions using the following formula: sum of 5 fields of view)/total number of stomata (sum of 5 fields of view) x 100.

Reporter lines: For confocal imaging, emerging 2nd (6-7 days post germination (dpg)) or 3rd (11-12 dpg) leaves from plants grown on plates were carefully pulled from the sheath of the older leaf to isolate and reveal the developmental leaf zone. Samples were stained in propidium iodide (PI, 1:100 of a 1 mg/ml stock) for 5 min to stain cell walls and/or mounted directly in water for imaging on a Leica SP8 confocal microscope (Leica Microsystems, Wetzlar, Germany). Image analysis was done using Fiji.

Total phenolics autofluorescence: Small leaf fragments previously fixed and cleared in 7:1 ethanol:acetic acid were washed in 70 % ethanol and then transferred to distilled water with 0.02 % (v/v) Tween for rehydration for 3 hours and mounted in distilled water for imaging. Samples were imaged on a Leica SP8 confocal microscope. Excitation and detection settings were as follows: Ex. 405 nm and Em. 490-550 nm. Laser power set to 10 %. For the analysis of PHCs, stacks of 0.33 µm steps were obtained and plot profile analysis was performed on sum slices Z-projections in Fiji. For the analysis of PHCs plot profiles, a straight line was drawn from the base of the PHCs to the tip and plot profiles of gray values were obtained. For the analysis of PHC average autofluorescence, PHCs were handtraced on the sum slices Z-projections and CTCF (corrected total cell fluorescence) calculated as Integrated Density – (Area of selected cell x Mean fluorescence of background readings). Mean fluorescence of 9 background readings per image were obtained to calculate CTCF (using the traced area at regions with only background signal) and to correct plot profiles. For the analysis of mature stomata autofluorescence, GCs were handtraced and autofluorescence was calculated as CTCF (corrected total cell fluorescence) = Integrated Density – (Area of selected cell x Mean fluorescence of background readings) from single images. Mean fluorescence of 3-4 background readings per image were obtained to calculate CTCF (using the traced area at regions with only background signal).

For the analysis of phenolic compounds during stomatal elongation (step 6i-6iii), the emerging 2nd (6-7 dpg) or 3rd (11-12 dpg) leaves were carefully pulled from the sheath of the older leaf to isolate and reveal the developmental leaf zone were mounted in water for imaging on a Leica SP8 confocal microscope. Autofluorescence intensity was measured on handtraced GCs from sum slices Z-projections (75 stacks) using Fiji and calculated as CTCF (corrected total cell fluorescence) = Integrated Density – (Area of selected cell x Mean fluorescence of background readings). Mean fluorescence of 3-4 background readings surrounding each stoma were obtained to calculate CTCF for each GC pair.

Basic fuchsin staining: Small leaf fragments previously fixed and cleared in 7:1 ethanol:acetic acid were transferred to distilled water with 0.02 % (v/v) Tween for rehydration for 3 hours. Samples were incubated in 30 µl of 0.01 % Basic Fuchsin (Sigma-Aldrich, St. Louis, Missouri, USA, Cat. no. 857343) for 5 min and washed twice with 30 µl of 50 % glycerol (v/v) for 5 min (2.5 min per wash step), and mounted in 50 % glycerol. Samples were imaged under Ex. 561 nm and Em. 573-603 nm. Stacks of 0.33 µm steps were obtained. For the analysis of PHCs, sum slices Z-projections were performed. A straight line was drawn from the base of the PHCs until the tip and plot profiles of gray values were obtained. Mean gray value of 9 back-

ground readings was obtained to correct each measurement. For the analysis of stomata, GCs were handtraced and fluorescence was calculated as CTCF (corrected total cell fluorescence) = Integrated Density − (Area of selected cell x Mean fluorescence of background readings) from single images. Mean fluorescence of 3-6 background readings was obtained for each image to calculate CTCF.

Safranin-o staining: Small leaf fragments previously fixed and cleared in 7:1 ethanol acetic acid were transferred to distilled water for 2 hours. Samples were incubated in 50 µl of 0.2 % Safranin-O (Sigma-Aldrich, St. Louis, Missouri, USA, Cat. no. 84120; v/v in 50 % EtOH) for 10 min, washed with 50 % EtOH for 10 min and hydrated in distilled water for 15 min. Samples were mounted in distilled water and imaged under Ex. 488 nm and Em. 530-560 nm (Channel 1 (C1)) and Ex. 561 nm and Em. 570-600 nm (Channel 2 (C2)). Stacks of 0.33 µm steps were obtained. A straight line was drawn from the base of the PHCs until the tip and plot profiles of gray values for C1 and C2 (same defined ROI) were obtained from the sum slices Z-projections. The ratio between the plot profiles from C2 and C1 was obtained. Additionally, images were analyzed using the Fiji macro developed by Baldacci-Cresp et al. 2020 for calculating a ratio from a generated ratiometric image (C2/C1) (Baldacci-Cresp et al., 2020).

REFERENCES

Abrash E, Anleu Gil MX, Matos JL, Bergmann DC. 2018. Conservation and divergence of YODA MAPKKK function in regulation of grass epidermal patterning. *Development* **145**:dev165860. doi:10.1242/dev.165860

Adrian J, Chang J, Ballenger CE, Bargmann BOR, Alassimone J, Davies KA, Lau OS, Matos JL, Hachez C, Lanctot A, Vatén A, Birnbaum KD, Bergmann DC. 2015. Transcriptome dynamics of the stomatal lineage: birth, amplification, and termination of a self-renewing population. *Dev Cell* **33**:107–118. doi:10.1016/j.devcel.2015.01.025

Allen GC, Flores-Vergara MA, Krasynanski S, Kumar S, Thompson WF. 2006. A modified protocol for rapid DNA isolation from plant tissues using cetyltrimethylammonium bromide. *Nat Protoc* **1**:2320–2325. doi:10.1038/nprot.2006.384

Andama JB, Mujiono K, Hojo Y, Shinya T, Galis I. 2020. Nonglandular silicified trichomes are essential for rice defense against chewing herbivores. *Plant Cell Environ* **43**:2019–2032. doi:10.1111/pce.13775

Angeles-Shim RB, Asano K, Takashi T, Shim J, Kuroha T, Ayano M, Ashikari M. 2012. A WUSCHEL-related homeobox 3B gene, depilous (dep), confers glabrousness of rice leaves and glumes. *Rice* **5**:28. doi:10.1186/1939-8433-5-28

Baldacci-Cresp F, Spriet C, Twyffels L, Blervacq A-S, Neutelings G, Baucher M, Hawkins S. 2020. A rapid and quantitative safranin-based fluorescent microscopy method to evaluate cell wall lignification. *Plant J* **102**:1074–1089. doi:10.1111/tpj.14675

Bond J, Donaldson L, Hill S, Hitchcock K. 2008. Safranine fluorescent staining of wood cell walls. *Biotech Histochem* **83**:161–171. doi:10.1080/10520290802373354

Burr SJ, Fry SC. 2009. Feruloylated arabinoxylans are oxidatively cross-linked by extracellular maize peroxidase but not by horseradish peroxidase. *Mol Plant* **2**:883–892. doi:10.1093/mp/ssp044

Cartwright HN, Humphries JA, Smith LG. 2009. PAN1: a receptor-like protein that promotes polarization of an asymmetric cell division in maize. *Science* **323**:649–651. doi:10.1126/science.1161686

Čermák T, Curtin SJ, Gil-Humanes J, Čegan R, Kono TJY, Konečná E, Belanto JJ, Starker CG, Mathre JW, Greenstein RL, Voytas DF. 2017. A Multipurpose Toolkit to Enable Advanced Genome Engineering in Plants. *Plant Cell* **29**:1196–1217. doi:10.1105/tpc.16.00922

Coomey JH, Sibout R, Hazen SP. 2020. Grass secondary cell walls, Brachypodium distachyon as a model for discovery. *New Phytol* **227**:1649–1667. doi:10.1111/nph.16603

de Boer HJ, Price CA, Wagner-Cremer F, Dekker SC, Franks PJ, Veneklaas EJ. 2016. Optimal allocation of leaf epidermal area for gas exchange. *New Phytol* **210**:1219–1228. doi:10.1111/nph.13929

Dittberner H, Korte A, Mettler-Altmann T, Weber APM, Monroe G, de Meaux J. 2018. Natural variation in stomata size contributes to the local adaptation of water-use efficiency in Arabidopsis thaliana. *Mol Ecol* **27**:4052–4065. doi:10.1111/mec.14838

Doheny-Adams T, Hunt L, Franks PJ, Beerling DJ, Gray JE. 2012. Genetic manipulation of stomatal density influences stomatal

size, plant growth and tolerance to restricted water supply across a growth carbon dioxide gradient. *Philos Trans R Soc Lond B Biol Sci* **367**:547–555.

Donaldson L. 2020. Autofluorescence in Plants. *Molecules* **25**:2393. doi:10.3390/molecules25102393

Dow GJ, Berry JA, Bergmann DC. 2014. The physiological importance of developmental mechanisms that enforce proper stomatal spacing in Arabidopsis thaliana. *New Phytol* **201**:1205–1217. doi:10.1111/nph.12586

Facette MR, Park Y, Sutimantanapi D, Luo A, Cartwright HN, Yang B, Bennett EJ, Sylvester AW, Smith LG. 2015. The SCAR/WAVE complex polarizes PAN receptors and promotes division asymmetry in maize. *Nat Plants* **1**:14024. doi:10.1038/nplants.2014.24

Fei S, Wenbin M, Hao W, Furong X, Chunyan X, Jianfei W. 2020. Paper New Allele of HL6 Regulates Trichome Elongation in Rice. *Rice Sci* **27**:480–492. doi:10.1016/j.rsci.2020.09.005

Franks PJ, Beerling DJ. 2009. Maximum leaf conductance driven by CO2 effects on stomatal size and density over geologic time. *Proc Natl Acad Sci U S A* **106**:10343–10347. doi:10.1073/pnas.0904209106

Franks PJ, Drake PL, Beerling DJ. 2009. Plasticity in maximum stomatal conductance constrained by negative correlation between stomatal size and density: an analysis usingEucalyptus globulus. *Plant Cell Environ* **32**:1737–1748. doi:10.1111/j.1365-3040.2009.002031.x

Franks PJ, Farquhar GD. 2007. The mechanical diversity of stomata and its significance in gas-exchange control. *Plant Physiol* **143**:78–87. doi:10.1104/pp.106.089367

Galdon-Armero J, Fullana-Pericas M, Mulet PA, Conesa MA, Martin C, Galmes J. 2018. The ratio of trichomes to stomata is associated with water use efficiency in Solanum lycopersicum (tomato). *Plant J* **96**:607–619. doi:10.1111/tpj.14055

García-Plazaola JI, Fernández-Marín B, Duke SO, Hernández A, López-Arbeloa F, Becerril JM. 2015. Autofluorescence: Biological functions and technical applications. *Plant Sci* **236**:136–145. doi:10.1016/j.plantsci.2015.03.010

González Moreno A, de Cózar A, Prieto P, Domínguez E, Heredia A. 2022. Radiationless mechanism of UV deactivation by cuticle phenolics in plants. *Nat Commun* **13**:1786. doi:10.1038/s41467-022-29460-9

Granier F, Lemaire A, Wang Y, LeBris P, Antelme S, Vogel J, Laudencia-Chingcuanco D, Sibout R. 2016. Chemical and Radiation Mutagenesis: Induction and Detection by Whole Genome Sequencing In: Vogel JP, editor. Genetics and Genomics of Brachypodium. Cham: Springer International Publishing. pp. 155–170. doi:10.1007/7397_2015_20

Haas A, Raissig M. 2020. Seed sterilization and seedling growth on plates in the model grass Brachypodium distachyon. *Bio Protoc* **10**:e3700. doi:10.21769/bioprotoc.3700

Hall CR, Dagg V, Waterman JM, Johnson SN. 2020. Silicon Alters Leaf Surface Morphology and Suppresses Insect Herbivory in a Model Grass Species. *Plants* **9**:643. doi:10.3390/plants9050643

Hatfield RD, Rancour DM, Marita JM. 2016. Grass Cell Walls: A Story of Cross-Linking. *Front Plant Sci* **7**:2056. doi:10.3389/fpls.2016.02056

Hoffmann N, Benske A, Betz H, Schuetz M, Samuels AL. 2020. Laccases and Peroxidases Co-Localize in Lignified Secondary Cell Walls throughout Stem Development. *Plant Physiol* **184**:806–822. doi:10.1104/pp.20.00473

Holzwart E, Huerta AI, Glöckner N, Garnelo Gómez B, Wanke F, Augustin S, Askani JC, Schürholz A-K, Harter K, Wolf S. 2018. BRI1 controls vascular cell fate in the Arabidopsis root through RLP44 and phytosulfokine signaling. *Proc Natl Acad Sci U S A* **115**:11838–11843. doi:10.1073/pnas.1814434115

Humphries JA, Vejlupkova Z, Luo A, Meeley RB, Sylvester AW, Fowler JE, Smith LG. 2011. ROP GTPases act with the receptor-like protein PAN1 to polarize asymmetric cell division in maize. *Plant Cell* **23**:2273–2284.

Jangra R, Brunetti SC, Wang X, Kaushik P, Gulick PJ, Foroud NA, Wang S, Lee JS. 2021. Duplicated antagonistic EPF peptides optimize grass stomatal initiation. *Development* **148**:dev199780. doi:10.1242/dev.199780

Javelle M, Vernoud V, Rogowsky PM, Ingram GC. 2011. Epidermis: the formation and functions of a fundamental plant tissue. *New Phytol* **189**:17–39. doi:10.1111/j.1469-8137.2010.03514.x

Kanaoka MM, Pillitteri LJ, Fujii H, Yoshida Y, Bogenschutz NL, Takabayashi J, Zhu J-K, Torii KU. 2008. SCREAM/ICE1 and SCREAM2 specify three cell-state transitional steps leading to arabidopsis stomatal differentiation. *Plant Cell* **20**:1775–1785.

Kapp N, Barnes WJ, Richard TL, Anderson CT. 2015. Imaging with the fluorogenic dye Basic Fuchsin reveals subcellular patterning and ecotype variation of lignification in Brachypodium distachyon. *J Exp Bot* **66**:4295–4304. doi:10.1093/jxb/erv158

Karabourniotis G, Liakopoulos G, Nikolopoulos D, Bresta P. 2020. Protective and defensive roles of non-glandular trichomes against multiple stresses: structure–function coordination. *Res J For* **31**:1–12. doi:10.1007/s11676-019-01034-4

Kong D, Pan X, Jing Y, Zhao Y, Duan Y, Yang J, Wang B, Liu Y, Shen R, Cao Y, Wu H, Wei H, Wang H. 2021. ZmSPL10/14/26 are required for epidermal hair cell fate specification on maize leaf. *New Phytol* **230**:1533–1549. doi:10.1111/nph.17293

Lampropoulos A, Sutikovic Z, Wenzl C, Maegele I, Lohmann JU, Forner J. 2013. GreenGate---a novel, versatile, and efficient cloning system for plant transgenesis. *PLoS One* **8**:e83043.

Lan T, Zheng Y, Su Z, Yu S, Song H, Zheng X, Lin G, Wu W. 2019. OsSPL10, a SBP-Box Gene, Plays a Dual Role in Salt Tolerance and Trichome Formation in Rice (Oryza sativa L.). *G3* **9**:4107–4114. doi:10.1534/g3.119.400700

Lawson T, Vialet-Chabrand S. 2019. Speedy stomata, photosynthesis and plant water use efficiency. *New Phytol* **221**:93–98. doi:10.1111/nph.15330

Le Bris P, Wang Y, Barbereau C, Antelme S, Cézard L, Legée F, D'Orlando A, Dalmais M, Bendahmane A, Schuetz M, Samuels L, Lapierre C, Sibout R. 2019. Inactivation of LACCASE8 and LACCASE5 genes in Brachypodium distachyon leads to severe decrease in lignin content and high increase in saccharification yield without impacting plant integrity. *Biotechnol Biofuels* **12**:181. doi:10.1186/s13068-019-1525-5

Li J, Tang B, Li Y, Li C, Guo M, Chen H, Han S, Li J, Lou Q, Sun W,

Wang P, Guo H, Ye W, Zhang Z, Zhang H, Yu S, Zhang L, Li Z. 2021. Rice SPL10 positively regulates trichome development through expression of HL6 and auxin-related genes. *J Integr Plant Biol* **63**:1521–1537. doi:10.1111/jipb.13140

Li Q, Hou J, He N, Xu L, Zhang Z. 2021. Changes in leaf stomatal traits of different aged temperate forest stands. *Res J For* **32**:927–936. doi:10.1007/s11676-020-01135-5

Liu T, Ohashi-Ito K, Bergmann DC. 2009. Orthologs of Arabidopsis thaliana stomatal bHLH genes and regulation of stomatal development in grasses. *Development* **136**:2265–2276.

Li X, Yang Y, Yao J, Chen G, Li X, Zhang Q, Wu C. 2009. FLEXIBLE CULM 1 encoding a cinnamyl-alcohol dehydrogenase controls culm mechanical strength in rice. *Plant Mol Biol* **69**:685–697. doi:10.1007/s11103-008-9448-8

McAusland L, Vialet-Chabrand S, Davey P, Baker NR, Brendel O, Lawson T. 2016. Effects of kinetics of light-induced stomatal responses on photosynthesis and water-use efficiency. *New Phytol* **211**:1209–1220. doi:10.1111/nph.14000

Nunes TDG, Slawinska MW, Lindner H, Raissig MT. 2022. Quantitative effects of environmental variation on stomatal anatomy and gas exchange in a grass model. *Quantitative Plant Biology* **3**:10.1017/qpb.2021.19. doi:10.1017/qpb.2021.19

Nunes TDG, Zhang D, Raissig MT. 2020. Form, development and function of grass stomata. *Plant J* **101**:780–799. doi:10.1111/tpj.14552

Raissig MT, Abrash E, Bettadapur A, Vogel JP, Bergmann DC. 2016. Grasses use an alternatively wired bHLH transcription factor network to establish stomatal identity. *Proc Natl Acad Sci U S A* **113**:8326–8331. doi:10.1073/pnas.1606728113

Raissig MT, Matos JL, Anleu Gil MX, Kornfeld A, Bettadapur A, Abrash E, Allison HR, Badgley G, Vogel JP, Berry JA, Bergmann DC. 2017. Mobile MUTE specifies subsidiary cells to build physiologically improved grass stomata. *Science* **355**:1215–1218. doi:10.1126/science.aal3254

Rancour DM, Marita JM, Hatfield RD. 2012. Cell wall composition throughout development for the model grass Brachypodium distachyon. *Front Plant Sci* **3**:266. doi:10.3389/fpls.2012.00266

Riglet L, Gatti S, Moyroud E. 2021. Sculpting the surface: Structural patterning of plant epidermis. *iScience* **24**:103346. doi:10.1016/j.isci.2021.103346

Rogers LA, Campbell MM. 2004. The genetic control of lignin deposition during plant growth and development. *New Phytol* **164**:17–30. doi:10.1111/j.1469-8137.2004.01143.x

Rojas-Murcia N, Hématy K, Lee Y, Emonet A, Ursache R, Fujita S, De Bellis D, Geldner N. 2020. High-order mutants reveal an essential requirement for peroxidases but not laccases in Casparian strip lignification. *Proc Natl Acad Sci U S A* **117**:29166–29177. doi:10.1073/pnas.2012728117

Schindelin J, Arganda-Carreras I, Frise E, Kaynig V, Longair M, Pietzsch T, Preibisch S, Rueden C, Saalfeld S, Schmid B, Tinevez J-Y, White DJ, Hartenstein V, Eliceiri K, Tomancak P, Cardona A. 2012. Fiji: an open-source platform for biological-image analysis. *Nat Methods* **9**:676–682.

Sexauer M, Shen D, Schön M, Andersen TG, Markmann K. 2021. Visualizing polymeric components that define distinct root barriers across plant lineages. *Development* **148**:dev199820. doi:10.1242/dev.199820

Sharma N. 2017. Leaf clearing protocol to observe stomata and other cells on leaf surface. *Bio Protoc* **7**:e2538. doi:10.21769/bioprotoc.2538

Shtein I, Shelef Y, Marom Z, Zelinger E, Schwartz A, Popper ZA, Bar-On B, Harpaz-Saad S. 2017. Stomatal cell wall composition: distinctive structural patterns associated with different phylogenetic groups. *Ann Bot* **119**:1021–1033. doi:10.1093/aob/mcw275

Sun W, Gao D, Xiong Y, Tang X, Xiao X, Wang C, Yu S. 2017. Hairy Leaf 6, an AP2/ERF Transcription Factor, Interacts with OsWOX3B and Regulates Trichome Formation in Rice. *Mol Plant* **10**:1417–1433. doi:10.1016/j.molp.2017.09.015

Sun Y, Yan F, Cui X, Liu F. 2014. Plasticity in stomatal size and density of potato leaves under different irrigation and phosphorus regimes. *J Plant Physiol* **171**:1248–1255. doi:10.1016/j.jplph.2014.06.002

Tokunaga N, Kaneta T, Sato S, Sato Y. 2009. Analysis of expression profiles of three peroxidase genes associated with lignification in Arabidopsis thaliana. *Physiol Plant* **136**:237–249. doi:10.1111/j.1399-3054.2009.01233.x

Torii KU. 2021. Stomatal development in the context of epidermal tissues. *Ann Bot* **128**:137–148. doi:10.1093/aob/mcab052

Ursache R, Andersen TG, Marhavý P, Geldner N. 2018. A protocol for combining fluorescent proteins with histological stains for diverse cell wall components. *Plant J* **93**:399–412. doi:10.1111/tpj.13784

Vogel J. 2008. Unique aspects of the grass cell wall. *Curr Opin Plant Biol* **11**:301–307. doi:10.1016/j.pbi.2008.03.002

Wang H, Guo S, Qiao X, Guo J, Li Z, Zhou Y, Bai S, Gao Z, Wang D, Wang P, Galbraith DW, Song C-P. 2019. BZU2/ZmMUTE controls symmetrical division of guard mother cell and specifies neighbor cell fate in maize. *PLoS Genet* **15**:e1008377. doi:10.1371/journal.pgen.1008377

Wang Y, Bouchabke-Coussa O, Lebris P, Antelme S, Soulhat C, Gineau E, Dalmais M, Bendahmane A, Morin H, Mouille G, Legée F, Cézard L, Lapierre C, Sibout R. 2015. LACCASE5 is required for lignification of the Brachypodium distachyon Culm. *Plant Physiol* **168**:192–204. doi:10.1104/pp.114.255489

Wu Z, Chen L, Yu Q, Zhou W, Gou X, Li J, Hou S. 2019. Multiple transcriptional factors control stomata development in rice. *New Phytol* **223**:220–232. doi:10.1111/nph.15766

Yan L, Cheng X, Jia R, Qin Q, Guan L, Du H, Hou S. 2014. New phenotypic characteristics of three tmm alleles in Arabidopsis thaliana. *Plant Cell Rep* **33**:719–731. doi:10.1007/s00299-014-1571-1

Zhang D, Abrash EB, Nunes TDG, Prados IH, Ximena Anleu Gil M, Jesenofsky B, Lindner H, Bergmann DC, Raissig MT. 2022. Opposite polarity programs regulate asymmetric subsidiary cell divisions in grasses. *bioRxiv*. doi:10.1101/2022.04.24.489281

Zhang L, Wang S, Yang X, Cui X, Niu H. 2021. An Intrinsic Geometric Constraint on Morphological Stomatal Traits. *Front Plant Sci* **12**:658702. doi:10.3389/fpls.2021.658702

Zhao D, Luan Y, Xia X, Shi W, Tang Y, Tao J. 2020. Lignin provides

mechanical support to herbaceous peony (Paeonia lactiflora Pall.) stems. *Hortic Res* **7**:213. doi:10.1038/s41438-020-00451-5

Zuch DT, Doyle SM, Majda M, Smith RS, Robert S, Torii KU. 2022. Cell biology of the leaf epidermis: Fate specification, morphogenesis, and coordination. *Plant Cell* **34**:209–227. doi:10.1093/plcell/koab250